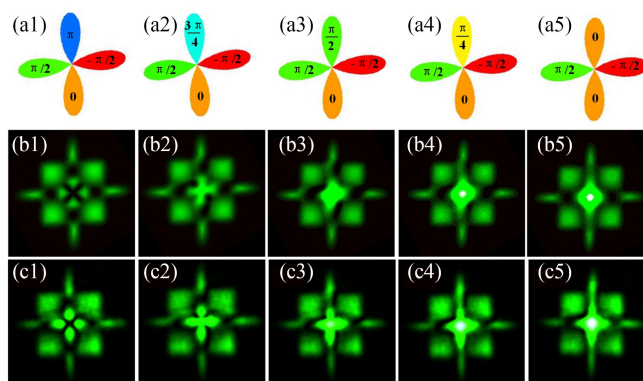


# Optical Image Self-Convolution Based on Second-Harmonic Generation With a Single Spatial Light Modulator

Volume 9, Number 6, December 2017

Fangshu Li  
Xiaodong Qiu  
Lixiang Chen



# Optical Image Self-Convolution Based on Second-Harmonic Generation With a Single Spatial Light Modulator

Fangshu Li, Xiaodong Qiu, and Lixiang Chen 

Department of Physics, Collaborative Innovation Center for Optoelectronic Semiconductors and Efficient Devices, Xiamen University, Xiamen 361005, China

DOI:10.1109/JPHOT.2017.2763740

1943-0655 © 2017 IEEE. Translations and content mining are permitted for academic research only.

Personal use is also permitted, but republication/redistribution requires IEEE permission.

See [http://www.ieee.org/publications\\_standards/publications/rights/index.html](http://www.ieee.org/publications_standards/publications/rights/index.html) for more information.

Manuscript received August 29, 2017; revised October 9, 2017; accepted October 12, 2017. Date of publication October 16, 2017; date of current version November 3, 2017. This work was supported in part by the National Natural Science Foundation of China (11474238, 91636109), in part by the Fundamental Research Funds for the Central Universities at Xiamen University (20720160040), in part by the Natural Science Foundation of Fujian Province of China for Distinguished Young Scientists (2015J06002), and in part by the program for New Century Excellent Talents in University of China (NCET-13-0495). Corresponding author: Lixiang Chen (e-mail: chenlx@xmu.edu.cn).

**Abstract:** By combining optical Fourier transform with second-harmonic generation (SHG) from infrared to visible region in a periodically poled Magnesium-doped Lithium Niobate (PPLN) crystal, we present a simple yet efficient experiment to revisit the optical implementation of image self-convolution. In contrast to previous scheme, here the main feature is the holographic gratings we prepare by a phase-only spatial light modulator that enables a deeper understanding on the centrosymmetry for intensity images, and particularly, the conjugate symmetry for both intensity and phase images. We manifest both cases by observing the real-time autocorrelation peaks that appear gradually in the output SHG signals. As our optical scheme possesses the inherent capacity of parallel processing, it will find potential in pattern recognition, particularly, for infrared remote sensing.

**Index Terms:** Optical self-convolution, second harmonic generation, symmetry, spatial light modulator

## 1. Introduction

Optical convolution and correlation have played a significant role in pattern recognition since they were proposed in 1962 by McLachlan [1]. In the beginning, optical pattern recognition was not actually appreciated until Lugi completed the complex spatial filter work in 1964 [2]. Two years later, the first joint transform correlator (JTC) architecture was demonstrated by Weaver and Goodman [3]. Then many applications based on these two traditional correlators appeared, but most of these experiments required computers to process images information [4]–[6]. Based on a magneto-optic device with a liquid crystal light valve, it was Yu and Lu who realized the real-time conventional JTC implementation [7]. The inherent advantage of using optical scheme to implement image convolutions is the parallel processing, which can reduce computational complexity and therefore accelerate the computing speed significantly. Ereemeeva *et al.* first combined second-order nonlinear optical effect with the Fourier optics to realize optical correlation, convolution, and self-convolution [8]. They subsequently realized the autocorrelation by method of four-frequency and two-stage three-frequency interactions [9]. Pepper *et al.* and White *et al.* demonstrated theoretically and

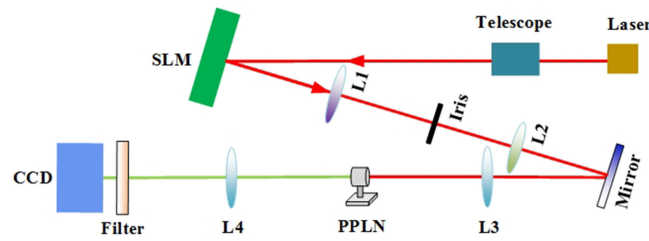


Fig. 1. Experimental setup for performing optical image self-convolution based on second harmonic generation with a single SLM.

experimentally that four-wave nonlinear mixing in photorefractive medium could be used for real-time convolution and correlation [10], [11]. Based on optical cross-correlation and self-convolution, Chiou *et al.* showed a fascinating applications of the selective enhancement of image components with specific symmetry [12]. Also, using anisotropic self-diffraction in BaTiO<sub>3</sub> crystals, Sun *et al.* developed a method to distinguish a centrosymmetric pattern from a noncentrosymmetric pattern with scale invariance [13].

In recent years, with the development of commercial spatial light modulators (SLM) [14], the computer-generated hologram offers an effective way to prepare and modulate a variety of phase masks for spatial filtering. For example, phase-only filters [15], binary phase-only filters [16], and amplitude-compensated filters [17], [18], were devised to improve the self-correlation efficiency. Here we combine the second harmonic generation (SHG) in the Fourier domain with a computer-controlled phase-only spatial light modulator (SLM) to revisit the experiment of optical image self-convolution. We employ a PPLN crystal to serve as the high-efficiency frequency doubler, and encode different complex amplitude images with SLM to prepare the input fundamental wave. Previous studies on optical self-convolution mainly focused on the real-amplitude intensity images, but the complex-amplitude, i.e., both intensity and phase images were rarely considered. The main feature in our scheme is the versatility of holographic gratings we prepare with SLM that enables a deeper understanding on the centrosymmetry for an intensity image, and particularly interestingly, the conjugate symmetry for a both intensity and phase image. We manifest both cases by observing the real-time autocorrelation peaks that appear gradually in the output SHG signals. Besides, the operating light fields converted from infrared wavelength to visible region may find some potential of our scheme in the infrared pattern recognition and remote sensing.

## 2. Experiment Scheme and Theoretical Model

Fig. 1 shows schematically our experimental setup. The light beam is derived from a 1064 nm laser source (Cobolt Rumba), and has a power of about 400 mW. After being collimated and expanded by a telescope, this fundamental frequency wave is incident on a SLM (Hamamatsu, X10468-07). The SLM is a reflective device, and the size of its screen is 16 mm × 12 mm consisting of 792 × 600 pixels with the pixel pitch of 20 μm, and each pixel imprints individually the incoming light with a phase modulation (0 ~ 2π). We assume the input original image is generally a both intensity and phase one, namely, whose complex amplitude can be described as,  $E_0(x_0, y_0) = A(x_0, y_0) \exp[i\varphi(x_0, y_0)]$ , where  $A(x_0, y_0)$  and  $\varphi(x_0, y_0)$  are the amplitude and phase distributions, respectively. We configure a single SLM as a diffractive component with a spatially dependent blazing function. The light propagating from the hologram has a phase profile,  $\varphi(x_0, y_0)$ , determined by the shape of the grating lines on the hologram, and an intensity pattern,  $A^2(x_0, y_0)$ , determined by their contrast. Generally, we can prepare the holograms displayed by the SLM according to the following equation [19]–[21]:

$$\Phi(x_0, y_0) = [\varphi(x_0, y_0) + \psi_L(x_0, y_0)_{\text{mod}2\pi} \times \text{sinc}^2(\pi[1 - A^2(x_0, y_0)])], \quad (1)$$

which appears as a product of the desired phase hologram with the desired intensity profile, specifically,  $\psi_L(x_0, y_0)$  is the phase of the linear blazed grating and  $\text{sinc}^2(\cdot)$  accounts for the mapping of the phase depth to the diffraction efficiency of the spatially dependent blazing function. Then a holographic grating is loaded on the screen of the SLM, the different orders of diffracted light are split after lens 1 and only the 1st-order diffracted light is used for imaging. Therefore, we filter out the image from the 1st-order diffraction by an iris through the first 4f optical system consisting of lens 1 and 2 ( $f_1 = 750$  mm and  $f_2 = 250$  mm). After the 4f system, the produced image at the mirror plane, see Fig. 1, is described by,

$$E_1(x_1, y_1) = A(-x_1, -y_1) \exp[i\psi(x_1, y_1)]. \quad (2)$$

We can see from Fig. 1 that there is another 4f optical system consisting of lens 3 and 4 ( $f_3 = 150$  mm and  $f_4 = 150$  mm) that is built to realize the optical self-convolution with the SHG effect in the Fourier domain. A 1 mm  $\times$  10 mm  $\times$  20 mm periodically poled Magnesium doped Lithium Niobate crystal (PPLN, Covision) is placed at the Fourier plane to serve as the frequency doubler. The PPLN crystal consists of five periods including 6.83  $\mu\text{m}$ , 6.86  $\mu\text{m}$ , 6.9  $\mu\text{m}$ , 6.93  $\mu\text{m}$ , 6.96  $\mu\text{m}$ , to realize the phase matching under different temperature. An oven is additionally used to control the temperature of the PPLN crystal at 73  $^\circ\text{C}$  in order to optimize the conversion efficiency [22], [23].

At the plane of PPLN, i.e., the rear focal plane of L3, we obtain the Fourier spectrum of the input image as,  $E_1(\xi, \eta) = \mathcal{F}\{E_1(x_1, y_1)\}$ , which plays the role of a fundamental wave to participate the SHG. The diffraction efficiency of SLM is about 5% such that we ensure the relatively low pump power to work under small signal approximation with an estimated SHG conversion efficiency only about 0.1%. Thus, under the paraxial condition, we can write the wave-coupling equations as [24],

$$\frac{d\tilde{E}_2(\xi, \eta)}{dz} = \frac{i\omega_2^2 d_{\text{eff}}}{\kappa_2 c^2} \tilde{E}_1(\xi, \eta) \tilde{E}_1(\xi, \eta) \exp(i \Delta \kappa z), \quad (3)$$

where  $d_{\text{eff}}$  is the effective nonlinear coefficient,  $z$  is the propagation distance, and  $\Delta \kappa = 2\kappa_1 - \kappa_2$  denotes the phase mismatching, with  $\kappa_1$  and  $\kappa_2$  being the wave vectors of fundamental frequency wave and second harmonic wave, respectively. Owing to phase matching independent of spatial distribution of a light field, under quasi phase matching condition in PPLN, namely,  $\Delta \kappa = 0$ , we know the input infrared 1064 nm light beam carrying the image information can be effectively converted to the 532 nm visible light beam [25]. From (3), we can derive the SHG light field at the Fourier plane as,

$$\tilde{E}_2(\xi, \eta) = \alpha \tilde{E}_1(\xi, \eta) \tilde{E}_1(\xi, \eta), \quad (4)$$

where  $\alpha = i\omega_2^2 d_{\text{eff}} L / (\kappa_2 c^2)$  and  $L$  is the length of PPLN crystal. The following lens L4 performs the Fourier transform on the SHG field,  $\tilde{E}_2(\xi, \eta)$ , then we obtain the output light field at the image plane of L4 as,

$$\begin{aligned} \tilde{E}_2(\xi, \eta) &= \alpha \mathcal{F}\{\tilde{E}_1(\xi, \eta) \tilde{E}_1(\xi, \eta)\} \\ &\propto E_0(x_0, y_0) * E_0(x_0, y_0), \end{aligned} \quad (5)$$

where  $*$  denotes the convolution operation, namely, for an arbitrary function  $g(x, y)$ , it is defined,

$$g(x, y) * g(x, y) = \int_{-\infty}^{\infty} g(\xi, \eta) g(x - \xi, y - \eta) d\xi d\eta. \quad (6)$$

In other words, the output 532 nm visible light field has acquired the self-convolution information of the input image encoded by the 1064 nm fundamental wave. After filtering and attenuating, we use a color CCD camera (Thorlabs, DCU224C) to record and monitor the output optical patterns in real time. In contrast to previous work, our scheme employs the computer-controlled versatile SLM that enables the investigation of optical self-convolution with a variety of complex amplitude images, e.g., both intensity and phase ones. Besides, as an important feature in the pattern recognition, it is critical to distinguish the specific spatial symmetry of two-dimensional images. And it was shown that self-convolution, instead of cross-correlation, could be used for the detection of this class of

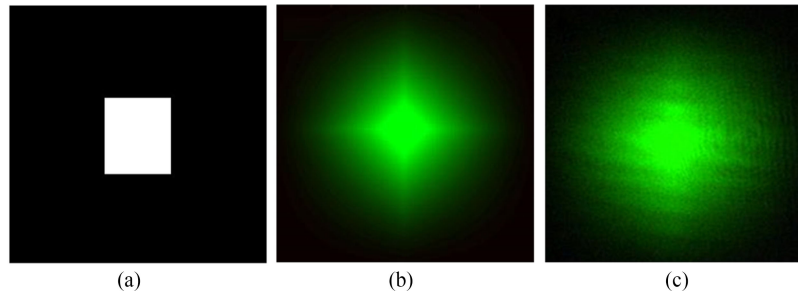


Fig. 2. (a) The input image of intensity rectangular aperture; (b) The simulation result; and (c) Experimental observation of the output SHG signals.

objects against others [12], [13], [26]. But their schemes were only applied to the real-amplitude images, not yet generalized to complex-amplitude images. In this regard, it deserves our attention to look at the relationship between self-convolution of (6) and auto-correlation, which is defined as,

$$g(x, y) \otimes g(x, y) = \int_{-\infty}^{\infty} g^*(\xi, \eta) g(x + \xi, y + \eta) d\xi d\eta, \quad (7)$$

where  $\otimes$  represents the correlation. A comparison between (6) and (7) leads to the conclusion that if  $g(x, y) \otimes g(x, y) = g^*(-x, -y) * g(x, y)$ , the auto-correlation and self-convolution are just equivalent. For intensity images, this describes the centrosymmetry, which has been extensively studied. However, there are still few studies to investigate the relevant conjugate symmetry for a both intensity and phase image. Here this forms the compelling reason for us to perform such an experiment.

### 3. Experiment Observations and Analysis

In our first set of experiment, we verify the effectiveness of our scheme by preparing an input image with a rectangular aperture, see Fig. 2(a). After self-convolution in the process of SHG at the Fourier plane, we obtain from (5) an analytical expression for the output light field as,

$$\begin{aligned} E_2(x_2, y_2) &= [\text{rect}(x_0)\text{rect}(y_0)] * [\text{rect}(x_0)\text{rect}(y_0)] \\ &= \mathcal{F}\{\text{sinc}^2(\xi)\text{sinc}^2(\eta)\} \\ &= \wedge(x_2) \wedge(y_2), \end{aligned} \quad (8)$$

where  $\text{sinc}^2(t) = \sin^2(t)/t^2$  and  $\wedge(t)$  is the triangular function. Based on (8) we present the simulation results in Fig. 2(b), where the output SHG light field appears as a two-dimensional triangular function. For comparison, we also show our experimental observation in Fig. 2(c), from which the good agreement can be seen clearly. Therefore this analytic case offers an intuitive result to confirm the good effectiveness of our scheme.

As mentioned before, the relationship between self-convolution and auto-correlation can be explored to investigate the centrosymmetry of an intensity image, and more generally, the conjugate symmetry of a both intensity and phase object. So in our second set of experiments, we demonstrate the gradual formation of auto-correlation peaks by manipulating the spatial symmetry of a Clover image. For observing the auto-correlation peak, we consider the pure intensity case, as is shown in Fig. 3. The top panel shows the input intensity Clover encoded in the 1064 nm fundamental wave, where we can see from left to right that the leftmost leaf grows from absolutely nothing to completely reproduction. One extreme case is the three-leaf clover of Fig. 3(a1), which lacks the centrosymmetry. In this case, the result of self-convolution cannot indicate any auto-correlation peak. The other extreme case is the whole four-leaf clover of Fig. 3(a5), whose centrosymmetry has been recovered. And we expect to observe a sharp auto-correlation peak by self-convolution in

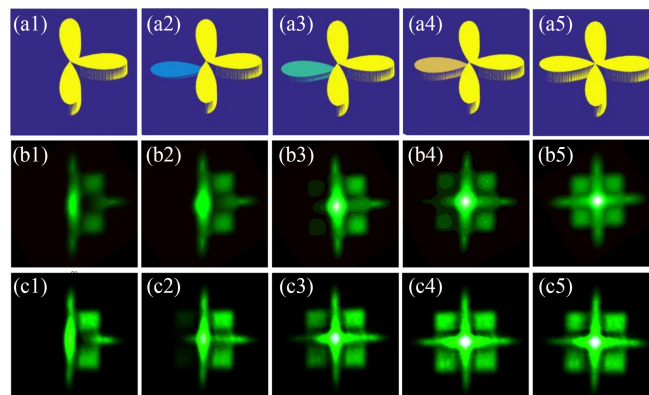


Fig. 3. Gradual formation of the auto-correlation peak arising from the centrosymmetry of an intensity Clover. Top panel: the input intensity Clover encoded in the invisible 1064 nm fundamental wave. Middle pane: the simulation results; Bottom panel: the experimental observations, see also the supplementary video 1.

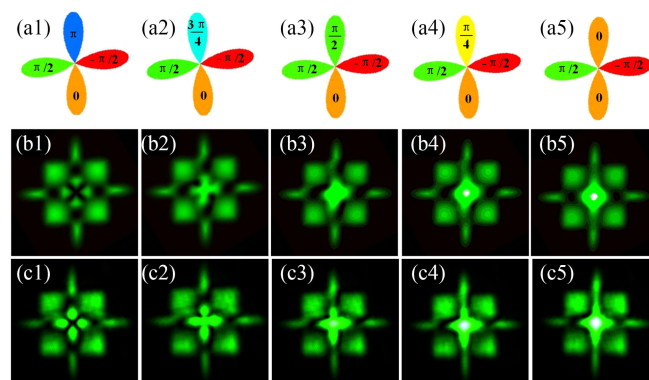


Fig. 4. Gradual formation of the auto-correlation peak arising from the conjugate symmetry of a both intensity and phase Clover. Top panel: the input both intensity and phase Clover encoded in the invisible 1064 nm fundamental wave. Middle panel: the simulation results; Bottom panel: the experimental observations, see also the supplementary video 2.

our scheme. Thus, we are able to demonstrate the gradual formation of the auto-correlation peak by simply changing the intensity of the most left leaf from zero to unit at an interval of 0.25. The middle and the bottom panel illustrate the corresponding numerical simulations and experimental results, respectively, which exhibits an excellent agreement. We indeed observe from left to right that there is an auto-correlation peak appearing gradually in the center of the output 532 nm pattern, as is recorded by the CCD camera. As the SLM is a reconfigurable diffractive hologram with a fresh rate of 60 Hz, we also present a supplementary video to show the real-time formation of auto-correlation peak.

In our further experiment, we investigate the conjugate symmetry for a both intensity and phase image, see the top panel in Fig. 4. The difference from the pure intensity image of Fig. 3(a5) is that here they share the same intensity profile but additionally we impart the four leaves with different phase values in a both intensity and phase Clover. In the top panel of Fig. 4, from left to right, we change only the phase value of one leaf from  $\pi$  to 0 at an interval of  $\pi/4$  while leave the phases of other three leaves remaining constant. Both the numerical simulations and experimental observations are presented in the middle and bottom panels, respectively, in Fig. 4. At first, for a phase-intensity four-leaf clover with phase distribution of  $1/2\pi$ , 0,  $-1/2\pi$ ,  $\pi$ , it lacks the conjugate-symmetry, see Fig. 4(a1). Thus we cannot observe an auto-correlation peak in the output SHG

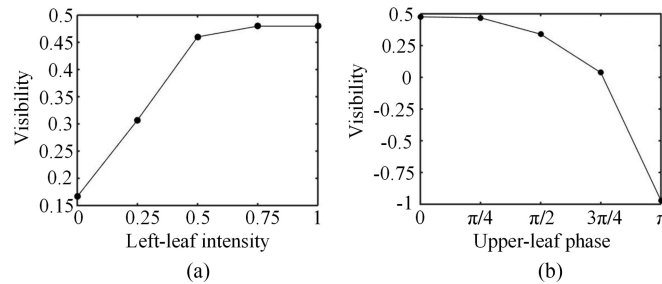


Fig. 5. The visibility of auto-correlation peaks: (a) an intensity Clover and (b) a both intensity and phase Clover.

signal, as was shown in both Figs. 4(b1) and 4(c1). In contrast, when the four-leaf clover possesses the phase distribution of  $1/2\pi$ ,  $0$ ,  $-1/2\pi$ ,  $0$ , satisfying the conjugate symmetry, see Fig. 4(a5), we can see that a sharp auto-correlation peak appears in both Fig. 4(b5) and 4(c5). Between these two extremes, the auto-correlation peak forms gradually, see also the supplemental video. We have also defined the visibility as,

$$V = \frac{P_{\text{main}} - P_{\text{sub}}}{P_{\text{main}} + P_{\text{sub}}}, \quad (9)$$

where  $P_{\text{main}}$  denotes the main power of auto-correlation peak and  $P_{\text{sub}}$  is the average power of the surrounding subpeaks. As is illustrated in Fig. 5, we can see that the visibility increases as the centrosymmetry of an intensity Clover (Fig. 3) or the conjugate symmetry of a both intensity and phase Clover (Fig. 4) is gradually formed, thus quantifying the degree of the centrosymmetry or conjugate symmetry.

## 4. Conclusion

In conclusion, we have combined the nonlinear optics of SHG effect with the Fourier transform to perform the optical self-convolution for a pure intensity image and a both intensity and phase image with the use of a single phase-only SLM. The experimental results recorded by a color CCD camera agreed well with the theoretical predictions. We revisited the centrosymmetry of an intensity clover image by observing the auto-correlation peak in the SHG signals. More generally, we demonstrated the conjugate symmetry for a both intensity and phase clover, and the gradual formation of auto-correlation peaks was recorded in real time. As our optical system possesses the inherent ability of parallel processing, the image conversion from invisible infrared illumination to visible green region suggests the potential in pattern recognition, particularly, for infrared remote sensing [27].

## References

- [1] D. McLachlan, "The role of optics in applying correlation functions to pattern recognition," *J. Opt. Soc. Amer.*, vol. 52, no. 4, pp. 454–459, 1962.
- [2] A. VanderLugt, "Signal detection by complex spatial filtering," *IEEE Trans. Inf. Theory*, vol. 10, no. 2, pp. 139–145, Apr. 1964.
- [3] C. S. Weaver and J. W. Goodman, "A technique for optically convolving two functions," *Appl. Opt.*, vol. 5, no. 7, pp. 1248–1249, 1966.
- [4] H. Stark, *Applications of Optical Fourier Transforms*. New York, NY, USA: Academic, pp. 67–81.
- [5] B. V. K. V. Kumar *et al.*, *Correlation Pattern Recognition*. Cambridge, U.K.: Cambridge Univ. Press, 2005.
- [6] M. S. Millan, "Advanced optical correlation and digital methods for pattern matching-50th anniversary of Vander Lugt matched filter," *J. Opt.*, vol. 14, no. 10, 2012, Art. no. 103001.
- [7] F. T. S. Yu and X. J. Lu, "A real-time programmable joint transform correlator," *Opt. Commun.*, vol. 52, no. 1, pp. 10–16, 1984.
- [8] R. A. Ereemeeva *et al.*, "Convolution and correlation of optical signals by nonlinear optics techniques," *Opt. Commun.*, vol. 5, no. 12, pp. 1429–1430, 1975.

- [9] R. A. Eremeeva, V. A. Kudryashov, I. N. Matveev, T. G. Usacheva, and A. I. Chekmenev, "Nonlinear optical methods for autocorrelation of objects," *Sov. J. Quantum Electron.*, vol. 7, no. 1, pp. 90–91, 1977.
- [10] D. M. Pepper *et al.*, "Spatial convolution and correlation of optical fields via degenerate four-wave mixing," *Opt. Lett.*, vol. 3, no. 1, pp. 7–9, 1978.
- [11] J. O. White *et al.*, "Realtime image processing via fourwave mixing in a photorefractive medium," *Appl. Phys. Lett.*, vol. 37, no. 1, pp. 5–7, 1980.
- [12] A. Chiou *et al.*, "Symmetry filters using optical correlation and convolution," *Opt. Eng.*, vol. 29, no. 9, pp. 1065–1072, 1990.
- [13] C. C. Sun *et al.*, "Optical symmetry filtering by use of anisotropic self-diffraction in BaTiO<sub>3</sub>," *Appl. Opt.*, vol. 38, no. 17, pp. 3720–3725, 1999.
- [14] N. Savage, "Digital spatial light modulators," *Nature Photon.*, vol. 3, no. 3, pp. 170–172, 2009.
- [15] J. L. Horner *et al.*, "Phase-only matched filtering," *Appl. Opt.*, vol. 23, no. 6, pp. 812–816, 1984.
- [16] D. Psaltis *et al.*, "Optical image correlation with a binary spatial light modulator," *Opt. Eng.*, vol. 23, no. 6, pp. 698–704, 1984.
- [17] G. G. Mu *et al.*, "Amplitude-compensated matched filtering," *Appl. Opt.*, vol. 27, no. 16, pp. 3461–3463, 1988.
- [18] M. A. Flavin *et al.*, "Amplitude encoded phase-only filters," *Appl. Opt.*, vol. 28, no. 9, pp. 1692–1696, 1989.
- [19] M. R. Dennis *et al.*, "Isolated optical vortex knots," *Nature Phys.*, vol. 6, no. 2, pp. 118–121, 2010.
- [20] W. Zhang *et al.*, "Mimicking faraday rotation to sort the orbital angular momentum of light," *Nature Phys.*, vol. 112, no. 15, 2014, Art. no. 153601.
- [21] C. Maurer *et al.*, "What spatial light modulators can do for optical microscopy," *Laser Photon.Rev.*, vol. 5, no. 1, pp. 81–101, 2011.
- [22] G. D. Miller *et al.*, "42%-efficient single-pass cw second-harmonic generation in periodically poled lithium niobate," *Opt. Lett.*, vol. 22, no. 24, pp. 1834–1836, 1997.
- [23] M. Zhou *et al.*, "52% optical-to-optical conversion efficiency in a compact 1.5 W 532 nm second harmonic generation laser with intracavity periodically-poled MgO:LiNbO<sub>3</sub>," *Opt. Lett.*, vol. 20, no. 7, pp. 1568–1571, 2010.
- [24] R. W. Boyd, *Nonlinear Optics*. New York, NY, USA: Academic, 2003.
- [25] Q. Zhou *et al.*, "Ultrasensitive mid-infrared up-conversion imaging at few-photon level," *Appl. Phys. Lett.*, vol. 102, no. 24, 2013, Art. no. 241110.
- [26] M. Novit *et al.*, "Similarities between self-convolution and symmetry mapping of multiplets in two-dimensional NMR spectra," *J. Magn. Reson.*, vol. 77, no. 2, pp. 394–400, 1988.
- [27] R. A. Schowengerdt, *Remote sensing: Models and methods for image processing*. New York, NY, USA: Academic, 1997.